Optical spectra and microscopic structure of the oxidized Si(100) surface: Combined *in situ* optical experiments and first principles calculations

Katalin Gaál-Nagy, Andrei Incze, and Giovanni Onida
Dipartimento di Fisica, Università di Milano, European Theoretical Spectroscopy Facility (ETSF), and CNISM-CNR-INFM, via Celoria 16, I-20133 Milano, Italy

Yves Borensztein, Nadine Witkowski, and Olivier Pluchery
Institut des Nanosciences de Paris, CNRS and University Pierre and Marie Curie, Paris 6, 140 rue de Lourmel, 75015 Paris, France

Frank Fuchs and Friedhelm Bechstedt
Institut für Festkörpertheorie und Optik, Friedrich-Schiller-Universität, Max-Wein-Platz 1, D-07743 Jena, Germany

Rodolfo Del Sole
Dipartimento di Fisica, Università di Roma "Tor Vergata," European Theoretical Spectroscopy Facility (ETSF), and CNR-INFM-SMC, via della Ricerca Scientifica, I-00133 Roma, Italy

(Received 31 July 2008; revised manuscript received 22 November 2008; published 21 January 2009)

We have investigated the first stages of the room-temperature oxidation of the Si(100) surface combining experimental surface optical spectra with the results of *ab initio* calculations. High-resolution reflectance anisotropy spectra (RAS) and surface differential reflectance spectra (SDRS) have been measured for the clean surfaces and various exposures up to 183 L, which have been compared with calculated RAS and SDRS in the independent-particle approximation. Our results, yielding a consistent description of both RAS and SDRS, suggest the coexistence of different structural domains, whose weight changes smoothly with the oxygen exposure. The main oxidation mechanisms together with their occurrence versus coverage are discussed.

DOI: 10.1103/PhysRevB.79.045312 PACS number(s): 78.68.+m, 73.20.−r, 78.40.−q

I. INTRODUCTION

The oxidation process of silicon surfaces, and particularly of the Si(100) surface, is of strong technological interest, driven by the downscaling of metal-oxide semiconductor devices. The latter requires nowadays gate insulator oxide layers with a thickness of less than 2 nm.[1] Even if new high-κ dielectric materials are explored,[2] Si oxidation continues to play a key role through the SiO_2-Si(100) interface formation. However, our understanding of the Si(100) oxidation process is still incomplete, particularly about its initial stages, which correspond to low-oxygen exposure and small coverages. Adsorption sites, surface structural changes, and oxygen reaction paths are still under debate.[3]

From the experimental point of view, optical reflectance anisotropy (RA) spectroscopy and surface differential reflectance (SDR) spectroscopies are two techniques which can be successfully used to investigate the oxidation process in real time.[4] RA and SDR spectroscopies are fast nondamaging techniques and can be easily performed "*in situ*" in a wide range of pressure and temperature. Besides other more direct techniques, optical measurements can be used to obtain structural information about surface reconstructions. However, this requires reliable theoretical predictions of the optical spectra for various surface geometries and stoichiometries. Such calculations can be performed within the *ab initio* density-functional theory Kohn-Sham (DFT-KS) (Refs. 5 and 6) scheme even for quite large and complex surface unit cells. For this reason, *ab initio* calculations associated with surface-sensitive linear optical techniques such as RA and SDR spectroscopies have become extensively used in the last years.

The clean Si(100) surface is a paradigmatic example for surface reconstructions. It reconstructs by dimerization of Si-Si pairs at the topmost surface layer by forming "dimer rows" in the direction perpendicular to the dimer axis. Adjacent rows of dimers are separated from each other by "valleys" which are about 2.67 Å wide. Due to the fact that the dimers are slightly buckled and that the buckling direction can alternate along one or both Cartesian directions in the surface plane, the surface periodicity can yield different reconstructions: besides the 2×1, also a $p(2\times2)$ and a $c(4\times2)$ reconstruction are observed.

At the clean Si(100) surface the Si-Si dimers, and the surface states related to them, have been recognized to be responsible for some spectral features in reflectance anisotropy spectra (RAS) and surface differential reflectance spectra (SDRS).[7] Optical techniques have been successfully employed also to study the adsorption of several atomic and molecular species including H, N_2O, C_6H_6, and O_2.[8–14] In the case of O_2, features in the SDRS of Si(100) at oxygen exposures of a few langmuirs (L) have been described considering a dissociative process and the breaking of surface dimers.[10,14] However, the way that oxidation influences the optical response is still not completely clarified.

On the other hand, the mechanism of the first stages of room-temperature oxidation of Si(100) has been studied in recent years with many different experimental techniques. Scanning reflection electron microscopy (SREM) combined with Auger-electron spectroscopy (AES) and core-level x-ray photoemission spectroscopy (XPS) have shown that Si(100) oxidation proceeds layer by layer[15] and that the first silicon layer is oxidized by molecular oxygen without an energy

barrier. High-resolution Rutherford backscattering spectroscopy (HRBS) has been used to monitor the oxygen depth profiles observed during the initial oxidation process.[16] After complete room-temperature oxidation, HRBS gives an oxygen coverage at saturation of ≈ 1.5 ML (monolayer). Oxygen atoms appear to be adsorbed mainly on the first silicon layer (including surface Si-Si dimers). During oxidation, the oxygen fraction in the second layer increases from less than 10% at 0.95 ML coverage to about 20% at 1.5 ML coverage. Other techniques such as photoelectron diffraction (PED),[17] core-electron photoemission spectroscopy (PES),[18] or time-resolved photoemission spectroscopy (TRPES) (Ref. 19) have been used to resolve the oxidation state of the Si atoms involved in bonding with oxygen, both at surface or interface, showing that a bridge-bond Si-O-Si model accounts for the structure at the interface.

An *in situ* combined scanning tunneling microscopy (STM) and scanning tunneling spectra (STS) study of the room-temperature oxide formation on Si(100)2×1 from molecular oxygen suggests that oxygen atoms adsorb initially on the back-bond sites of the surface dimers.[20] STM shows that even at 4.5 L exposure, the Si(100)2×1 dimer structure is still observed probably because of the survival of unoxidized surface dimers. Oxidizing at 15 L shows instead that the surface is completely covered with oxide. A more recent STM study of Si(100)2×1 oxidation by ozone—even if long-range oxidation patterns can be different in this case from those obtained with molecular oxygen—shows that in the initial oxidation stage the bridge site on the surface dimers and the backbonds of Si atoms of the dimers are the most favorable adsorption sites.[21] These observations are confirmed by *ab initio* total-energy calculations, performed by several authors using density-functional theory-local-density approximation/generalized gradient approximation (DFT-LDA/GGA)[22–24] or quantum-chemistry methods.[25,26] A spin-polarized first principles molecular-dynamics calculation by Ciacchi *et al.*[3] applied to the native oxide growth on Si(100) shows that the initial oxidation process is barrierless and, in a sense, "autocatalytic," and it is hence expected to proceed via the fast formation of a large number of patch such as agglomerates of oxide species distributed randomly, as has been suggested on the basis of a number of experimental investigations.[27,28] Ciacchi *et al.*[3] also indicated that after the spontaneous dissociation of an O_2 molecule, oxygen atoms can remain trapped both on a dimer or on a dimer backbond site, particularly the two oxygen atoms can even go on two adjacent surface dimers. At oxygen coverages of about 1.5 ML they show that there are very few narrow channels for spontaneous oxidation and that there are no reactive sites present at the outer surface.

The situation can be quite different in the case of high-temperature oxidation, such as in the experiments performed by Yasuda *et al.*[29] and Albao *et al.*[30] In fact, it has been proposed that the high temperature of the substrate ($\geq$800 K) makes the oxidation process a more complex phenomenon than the simple dissociative adsorption of O_2 at the surface followed by diffusion at and under the surface. Indeed, above 800 K the lifetime of adsorbed oxygen is short since SiO desorption is rapid, and etching of the surface or "active oxidation" is the main process.[31–33] The morphology of the surface becomes more complicated than in the case of room-temperature "passive" oxidation: a "quasi-layer-by-layer" etching of the surface occurs, as the vacancies created by SiO desorption aggregate into monolayer-deep elliptical etch pits.[33] Nevertheless, it is also found that in the temperature range between 853 and 913 K the oxidation still follows the exponential Langmuir rule.[13]

However, good experimental data for optical spectra as a function of the oxygen coverage are still lacking, especially in the case of SDR. Which oxidation mechanism is responsible for the change in optical spectra remains an open question, calling for new high-resolution experiments together with a comprehensive theoretical description.

In this work, we present and analyze room-temperature *in situ* RA and SDR measurements on a nominal Si(100)2×1 surface, performed for exposures ranging from sublangmuir to hundreds of langmuirs. These data are analyzed in association with *ab initio* calculations of the optical spectra, in order to get more insight on the oxidation process, particularly in its initial stages.

This paper is organized as follows: after a brief review of the general framework, both from the experimental and theoretical points of view (Secs. II and III), we present and qualitatively interpret sets of experimental RAS and SDRS, measured as a function of the oxygen exposure in Sec. IV. In Sec. IV A, theoretical predictions for structural properties of the clean and some of the lowest-energy configurations of the Si(100):O surface are described. In addition, the behavior of the Kohn-Sham (KS) band structure is studied for the oxidized structures, highlighting the effect of the oxidation on the dimer-dimer interaction and the dispersion of related surface bands. In Sec. IV B the basis of our study, i.e., the measured and calculated RAS spectra at various coverages, are presented. These spectra are then used for the interpretation of experimental data at increasing oxygen exposure for the RA at low coverage in Sec. IV C. Here, also the evolution of the coverage and mixing of different reconstructions for various exposures is discussed. Next, this mixing is used to predict theoretical SDRS which are compared with the measured ones in Sec. IV D. In Sec. IV E, the high-coverage case is investigated in a similar manner. Finally, we draw some conclusions (Sec. V).

II. EXPERIMENTAL SETUP

The experiments were carried out in an ultrahigh vacuum (UHV) preparation chamber with a base pressure of 5×10^{-11} Torr, equipped with low-energy electron diffraction, RAS and SDRS apparatus. The silicon samples were highly oriented (100) wafers, phosphorus-doped with a resistivity of 0.1–1 Ω cm. They were cleaned and reconstructed by direct continuous current heating up to 1323 K. As shown previously,[34] this procedure induces electromigration of the Si atoms at the surface, and it leads to the formation of a single-domain nominal (1×2) surface, constituted of large majority (1×2) domains separated by double steps and minority (2×1) domains. Oxygen was introduced by the use of a precision leak valve, its purity was checked with a mass spectrometer and the exposure was monitored with a Bayard-

Alpert-type ion gauge located in the pumping well far away from the sample to prevent atomic oxygen contamination. All the optical measurements were performed at room temperature by use of a home-made apparatus. The RAS apparatus is similar to the one developed by Aspnes *et al.*[35] For SDRS, we used a spectrometer based on an optical multichannel analyzer consisting of a Si photodiode array, as described in detail in Ref. 36.

III. THEORY

Ground-state and relaxed equilibrium geometries for the clean and oxidized surfaces were computed in a standard way within DFT, using a plane-waves basis set. All-electron-like wave functions are generated for the valence electrons within the projector-augmented wave (PAW) method. The excited states have been computed in the independent-particle approximation, using KS eigenvalues and eigenvectors as a starting point, and neglecting both self-energy and excitonic effects.[37] The computational details have been the same as those of Ref. 38; in particular, KS wave functions have been expanded up to an energy cutoff of 30 Ry. In the calculation of the dielectric response, we apply an upward, rigid energy shift of 0.5 eV to all the optical spectra (scissor operator), as the standard zeroth-order approximation to keep into account all neglected self-energy and many-body effects.[39]

Finally, we proceed to the calculation of the RA, defined as the real part of the difference between (normalized) complex reflectances in amplitude measured at normal incidence, $\mathrm{Re}(\Delta r/r)$, for two orthogonal polarizations of light. In our case, we distinguish the two polarizations, along the $[\bar{1}10]$ (x) and the $[110]$ (y) direction, which are parallel ($\parallel$) or perpendicular ($\perp$) to the Si-Si dimers, respectively. As the reflectivity R is equal to the square of the complex reflectance r, the RA can be written, as a function of the photon energy ω, as $I_{\mathrm{RA}}(\omega)=1/2[(\Delta R_{\parallel}/R_0)-(\Delta R_{\perp}/R_0)]$, where $\Delta R=(R-R_0)$, with R_0 being the (isotropic) Fresnel reflectivity. Describing the surface within a symmetric slab geometry, one can express $\Delta R_i/R$, for normally incident light, as[40]

$$\frac{\Delta R_i}{R}=\frac{4\omega}{c}\mathrm{Im}\frac{4\pi\alpha_{ii}^{\mathrm{hs}}(\omega)}{\epsilon_b(\omega)-1}, \tag{1}$$

where i is the polarization direction, $\alpha_{ii}^{\mathrm{hs}}(\omega)$ are the complex diagonal terms of the half-slab polarizability tensor, and $\epsilon_b(\omega)$ is the complex bulk dielectric function.

The imaginary part of $\alpha_{ii}(\omega)$ can be written in the single-quasiparticle approximation as

$$\mathrm{Im}[4\pi\alpha_{ii}(\omega)]=\frac{8\pi^2e^2}{\omega^2A}\sum_{\mathbf{k}}\sum_{v,c}|V_{v\mathbf{k},c\mathbf{k}}^{i}|^2\delta(E_{c\mathbf{k}}-E_{v\mathbf{k}}-\hbar\omega), \tag{2}$$

where $V_{v\mathbf{k},c\mathbf{k}}^{i}$ are the matrix elements of the velocity operator between occupied (v) and empty (c) slab eigenstates at the point $\mathbf{k}$ in the surface Brillouin zone,[41] A is the surface area, while $E_{c\mathbf{k}}$ and $E_{v\mathbf{k}}$ are conduction and valence energy eigenvalues, taken as KS eigenenergies. Neglecting the pseudopotential nonlocality,[42] the velocity operator can be replaced by the momentum operator divided by the electronic mass, whose matrix elements $P_{v\mathbf{k},c\mathbf{k}}^{i}$ are easy to evaluate in the plane-wave basis. Similarly, the SDR measures the reflectance difference between the clean and the oxidized surface,

$$I_{\mathrm{SDR}}=\frac{\Delta R_{\mathrm{clean}}}{R_0}-\frac{\Delta R_{\mathrm{oxidized}}}{R_0}, \tag{3}$$

and can be measured either with polarized or unpolarized light.

IV. RESULTS

We investigate the evolution of the RAS and the SDRS from both the experimental and theoretical points of view. In a first step, we analyze various possible surface reconstructions and the corresponding electronic band structure (Sec. IV A). For all these structures we have calculated the RAS

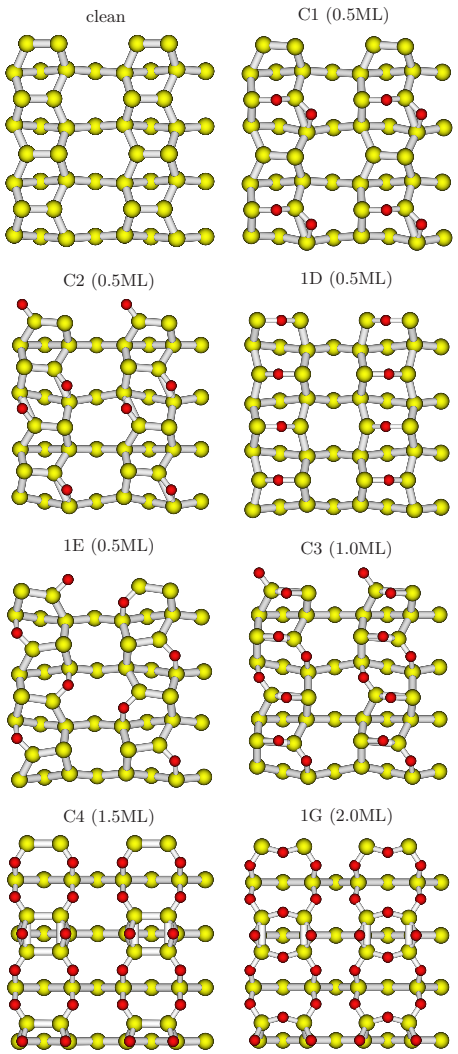

FIG. 1. (Color online) Surface structures (shown for convenience using a 4×4 surface cell) of the clean and oxidized Si(100) from top to bottom and from left to right with increasing oxygen coverage. Structures 1D, 1E, and 1G are from Ref. 38; clean and C1 are from Ref. 43.

TABLE I. Evolution of the structural properties related to surface dimers with increasing oxygen coverage. Subscripts index the two surface dimers contained in the (2×2) unit cell. α_1 and α_2 are the buckling angles (in degrees) of the two dimers in the unit cell, d_1 and d_2 are the Si-Si distances, and d_3 is the distance between the dimer down-atom and the next nondimer neighbor, the preferred oxygen adsorption side (see Fig. 1). In case of oxygen adsorption there, the length of this bond is given in the table.

Surface	α_1	d_1 (Å)	α_2	d_2 (Å)	d_3 (Å)
Clean	18.7	2.36	18.7	2.36	2.35
C1 (0.5 ML)	10.6	3.16	20.1	2.37	2.79
C2 (0.5 ML)	16.3	2.33	16.4	2.33	2.82
1D (0.5 ML)	17.3	3.24	17.3	3.24	2.32
1E (0.5 ML)	15.8	2.34	15.8	2.34	2.93
C3 (1.0 ML)	12.7	3.19	12.7	3.19	2.78
C4 (1.5 ML)	0.0	2.40	0.0	2.40	2.91
1G (2.0 ML)	0.0	3.05	0.0	3.05	2.90

spectra, which are presented in comparison with the measured data (Sec. IV B). This comparison guides the choice of the most probable reconstructions, whose spectra are used to fit the experimental data, where a mixing of various reconstructions is used for the low-coverage RA spectra (Sec. IV C). From the resulting mixing coefficients we predict the low-coverage SDR curves, which are shown in Sec. IV D in comparison with the experimental results. The high-coverage RAS and SDRS are discussed in Sec. IV E.

A. Model structures and electronic band structure

From the theoretical point of view, several low-energy configurations of oxidized Si(100) have been considered. We used either $p(2\times2)$ or $c(4\times2)$ unit cells since from the structural point of view, the difference between a $p(2\times2)$ and a $c(4\times2)$ surface is just in the buckling alternation along the direction perpendicular to the dimer rows (i.e., parallel to the dimers).[43] Only the oxidation of the topmost silicon layers is considered, corresponding to coverages up to 2.0 ML. Figure 1 displays the corresponding atomic positions after structural relaxation. The considered structures correspond to a subset of those presented in Ref. 38 (labeled as 1D, 1E, and 1G, respectively), plus the structure at 0.5 ML considered in Ref. 43 (here labeled as C1), and three other low-energy equilibrium structures (labeled as C2, C3, and C4, respectively). All structures involve oxidation of Si atoms of the topmost layer, with oxygen adsorbed either on Si-Si dimers, on dimer backbonds, or on both. In particular, structure C1 has an oxygen atom in bridge position onto one of the two Si-Si dimers of the $p(2\times2)$ unit cell, and a second oxygen (which we assume to originate from the dissociation of an impinging O_2 molecule) lying on the backbond position of the "low" atom of the same dimer. This position has been shown to be one of the lowest-energy minima for a 0.5 ML coverage.[44] An alternative minimum, corresponding to the same coverage, is that corresponding to structure C2, where the two O atoms occupy backbond positions on the low ends of both dimers, while dimer bonds themselves have no oxygen in the bridge position. Two other possibilities for a 0.5 ML coverage are those labeled as 1D and 1E in Ref. 38, and reproduced in Fig. 1. Structure 1D has oxygen only on dimer bridge positions, and is suggested by a recent total-energy calculation using (spin-polarized) GGA,[45] where this geometry is found as a result from the spontaneous dissociation of an O_2 molecule impinging perpendicularly to the surface dimers. Its stability is also confirmed in a recent work by Takahashi *et al.*[46] The structure 1E, which is found to be just 0.08 eV/atom more stable than 1D,[44] is similar to C2 (oxygen only on backbonds), but it has the oxidized bonds pointing in different directions. The three remaining structures, labeled as C3, C4, and 1G, correspond to higher coverages (two, three, and four O_2 molecules per (2×2) cell, respectively). Our structure C4 coincides with the structure "6*c*" in Ref. 47. An alternative structure at the same coverage (1.5 ML), obtained from C3 by oxidizing all the remaining backbonds (and yielding a ring of Si-O-Si-O bonds) has been discarded since it corresponds to a total energy 0.35 eV/atom higher than C4. Note that the oxygen adsorption energies (per oxygen atom) for C1 (6.57 eV), C2 (6.62 eV), 1D (6.49 eV), 1E (6.57 eV), C3 (6.56 eV), C4 (6.88 eV), and 1G (7.13 eV) are in general very similar.

Figure 1 also shows the important relaxations which occur at the surface: in general, the insertion of oxygen pushes away the neighboring Si atoms, both for the insertion of oxygen at dimers or backbonds. The largest effects are seen in the case of C4, where adjacent dimers are shown to regroup in pairs, bridged transversely by oxygen atoms. Looking at the dimer buckling, one sees a decrease at increasing coverage, with the dimers becoming essentially unbuckled at oxygen saturation (see Table I).

Structural changes are accompanied by quite large modifications of the electronic band structure with respect to the one of the clean surface (see Fig. 2). As a general rule, oxygen insertion strongly perturbs the dimer-dimer interaction, changing the dispersion of surface bands related to them. As already noticed in Ref. 43, the clean surface is characterized by a dimer-related band which is strongly dispersive in the direction of the dimer chains (i.e., perpendicularly to the

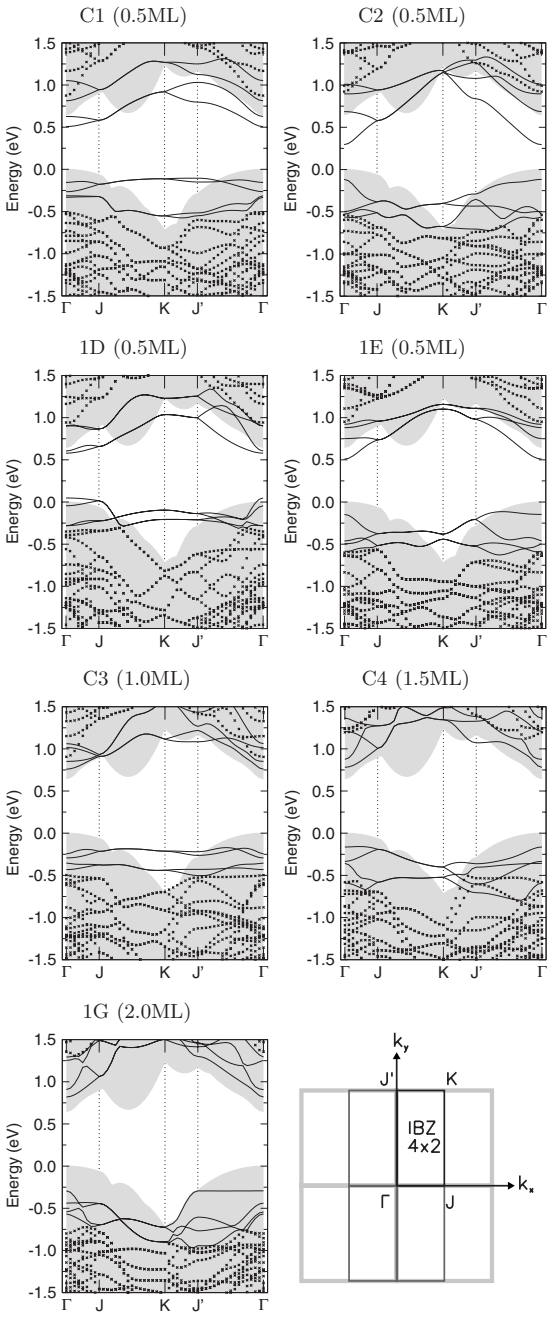

FIG. 2. KS band structures for the oxidized configurations shown in Fig. 1. The directions are indicated in the scheme of the surface irreducible Brillouin zone (IBZ). The JK direction is parallel while the ΓJ one is perpendicular to the surface dimers (see text). The shaded regions mark the projected bulk bands, the dots indicate the calculated slab eigenstates, and solid lines are used to denote surface states.

dimer axis $\Gamma J'$ or JK). This band flattens whenever the dimers are oxidized (as, e.g., in models C1 and C3). On the other hand, the dispersion in the direction parallel to the dimer axis (ΓJ or $J'K$) is generally increased by the oxidation (see, e.g., the models C2 and 1E). As a final result, in the oxidized surfaces the dispersion of surface bands is similar in both directions.

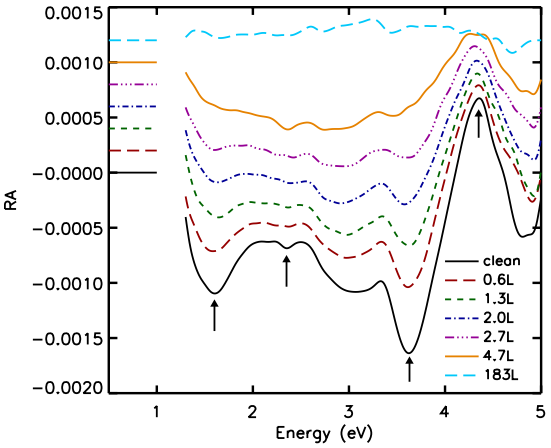

FIG. 3. (Color online) Experimental RAS of Si(100) for various oxygen exposures, smoothed by a Gaussian convolution using a broadening of 0.05 eV. The spectra are shifted upwards in steps of 0.0002 with respect to the clean surface curve, to which the vertical axis is referred, the corresponding zero lines are drawn next to the graph. The arrows indicate the four peaks entering the fitting procedure (see text).

B. Experimental and theoretical RAS

The complete set of experimental RAS for increasing exposures to molecular oxygen, from 0 to 183 L, is presented in Fig. 3. The RAS of the clean surface is similar to what has been measured previously, either by a similar procedure[12,34] or by a strain-based one,[48] with the typical double feature at 3.6–4.3 eV and the dimer-related surface-state transition at 1.6 eV. The intensity of the RA depends not only on the quality of the surface but mainly on the ratio between 1×2 and 2×1 domains. We have checked actually that, although this ratio does not influence the shape of the curve, it can change its intensity by a factor of about three. The shape of the spectra progressively changes from the one of the clean surface to an almost completely quenched RA signal, obtained for a largely oxidized surface (183 L). The surface-to surface-state transition (from the π-like to the π^*-like states of the Si dimers delocalized along the dimer rows, as discussed below), observed at 1.6 eV, is quickly removed and it almost disappears for 2 L, although an overall anisotropy with the double structure at 3.7–4.3 eV is still visible. This faster decrease in the 1.6 eV surface transition can be understood by the fact that the corresponding surface states are extremely sensitive to the cleanliness or to the crystallinity of the surface. For example, this transition is almost not visible for clean single-domain vicinal surfaces, where the 1×2 domains extend over 4 nm only.[12] Such a limited extension of the terraces strongly broadens the low-energy structures.

In Fig. 4 we report the RAS predicted for all considered geometries, separating the low-coverage structures (i.e., clean, C1, C2, 1D, and 1E) from the higher-coverage ones (C3, C4, and 1G). The RAS of the clean surface is also shown for comparison. The changes in the electronic structure are, in turn, reflected into the resulting theoretical optical spectra. Almost for every surface reconstruction, the surface anisotropy is reduced in the oxidized surfaces, which is consistent with the similarity of the dispersion in the surface

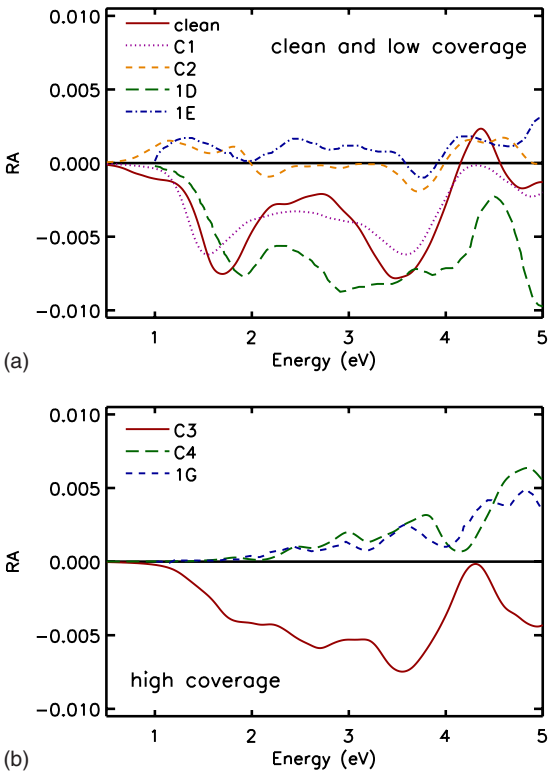

FIG. 4. (Color online) Upper panel: Theoretical RA of the clean and 0.5 ML coverage structures. Lower panel: Theoretical RA of structures with oxygen coverage larger than 0.5 ML. (See Fig. 1.)

bands (see Fig. 2). It can be noticed that the spectrum for the C1 structure is very similar to the clean surface one. In all other cases, different structures give substantially different spectra concerning peak structures and sign of anisotropy, and neither of the considered models alone turns out to be able to reproduce satisfactorily the experimental results for both RA and SDR, especially in the low-coverage regime. This becomes evident from the experimental spectra, shown in Fig. 3. In particular one can notice, besides a global RA reduction discussed above, the survival (up to 5 L) of an almost constant negative contribution in the 2.0–3.5 eV range. This suggests an important 1D contribution (see Fig. 4).

C. RAS for the clean surface and the low-coverage regime

Due to the fact that at low coverage many configurations with a similar total energy are possible, it seems, however, more realistic to propose a surface model consisting in a mixture of different domains, where all (or some) of the well-defined low-energy structural models (0.5 ML ones and clean) are represented. We notice that: (i) recent STM/STS experiments on Si(100)2×1 oxidized by molecular oxygen at room temperature show that even at 4.5 L exposure, some unoxidized (clean) domains persist at the surface;[20] (ii) structures C2 and 1E, where all dimers have an oxidized backbond, give rise to a similar (quenched) RAS; a clear distinction between the two backbond configurations is therefore not possible from the present results; (iii) the C1 structure gives a RAS very similar to the one of the clean surface,[43] as shown in Fig. 4, while experiments show an appreciable change already for 0.6 L (see Fig. 3); and (iv) the RAS of the 1D structure shows negative contributions in the region between 2 and 3 eV, in agreement with experimental data for oxidized surfaces. For the above reasons, we consider a four-component model assuming a mixture of the latter (1D) structure, plus the 1E and the C1 structure, and a possible contribution from clean surface domains. The above mixture is assumed to be representative of contributions coming from oxygen in dimers (structure 1D), oxygen in backbonds (structure 1E, which from our discussion is indistinguishable from the C2 one), and oxygen in mixed configurations (structure C1). Assuming this four-component model, we describe the RAS as a linear combination,

$$I_{\mathrm{RA}} = x_{\mathrm{D}} I_{\mathrm{RA}}^{\mathrm{1D}} + x_{\mathrm{E}} I_{\mathrm{RA}}^{\mathrm{1E}} + x_{\mathrm{C}} I_{\mathrm{RA}}^{\mathrm{C1}} + (1 - x_{\mathrm{D}} - x_{\mathrm{E}} - x_{\mathrm{C}}) I_{\mathrm{RA}}^{\mathrm{clean}}, \tag{4}$$

where the coefficients x_{D}, x_{E}, and x_{C} vary between 0 and 1 and are determined by a least-squares fit to the main peaks of the experimental RAS for the different exposures as indicated in Fig. 3.

In a first step, we compare the calculated RAS for the clean surface to the experimental spectrum, which is drawn in the top panel of Fig. 5. At this point, it must be noticed that theoretical RAS are usually overestimated with respect to experiment because of disorder and of minority domains at the clean surface.[7,49] Consequently, the theoretical spectrum has been divided by a factor of 4.8, for comparison with the experiment, which is in the range of other reported ones.[7,49] This scaling factor is taken as a fixed value for the following fittings of the oxidized surface RAS since we assume that this situation is not changed during the oxidation process. The overall agreement for the clean surface (Fig. 5) is good, particularly for the main negative and positive features at 3.6–4.3 eV. The surface-to-surface state transition at 1.6 eV is also quite well reproduced by the calculation. The latter transition occurs from the occupied π-like surface band to the empty π^*-like one, both localized on Si dimers and extending along the dimer rows, as discussed below. The relative intensity of the 1.6 eV minimum in the experiment is smaller than in the calculation, which is likely due to defects at the surface such as steps, which are known to strongly affect this intensity.

In a second step, we fit the parameters x_{C}, x_{D}, and x_{E} by using Eq. (4) in order to reproduce the experimental RA spectra drawn in Fig. 5 for increasing amounts of oxygen. The parameters x_{D} and x_{E} are shown in Fig. 6, while x_{C} is kept equal to zero. The insertion or exclusion of the C1 structure from the fit shown in Fig. 5 is a delicate point that we have seriously considered. The extension of C1 domains is of course zero before the oxidation starts, and the initial fits (performed taken into account C1) yields zero up to 2 L. For 4.7 L, the RAS line shape shown in Fig. 3 suggests that C1, if any, is very small. For these reasons, after a reasonable interpolation, we exclude C1 for the whole range 0–4.7 L. On the contrary, the fitting procedure shows that "clean surface" domains are present, even up to 4.7 L. The "clean"

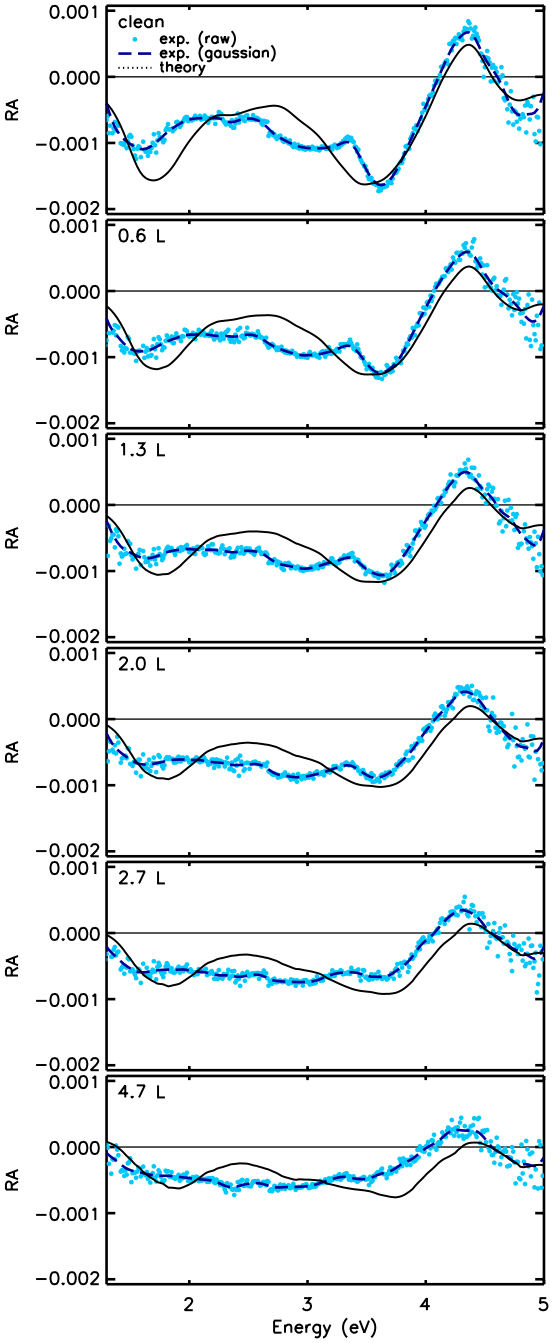

FIG. 5. (Color online) Comparison of the experimental RA data (dots and dashed line) with the fitted theoretical curves obtained from Eq. (4) (see text) including the structures 1D+1E+clean (solid line). The dashed lines correspond to the lines in Fig. 3.

areas are of course 100% before the oxidation starts, then they decrease smoothly, down to less than 0.1 ML at 4.7 L (see Fig. 6). Their presence at about 4.5 L is seen also in the STM/STS measurements of Ref. 20. Hence we keep clean surface domains in the fit of Fig. 5.

The resulting, theoretical RA curves for increasing amounts of oxygen are shown by the full lines in Fig. 5, in comparison with the RA experimental data. The overall agreement is satisfactory in the whole energy range. The discrepancy in the range between 2 and 3 eV can be further

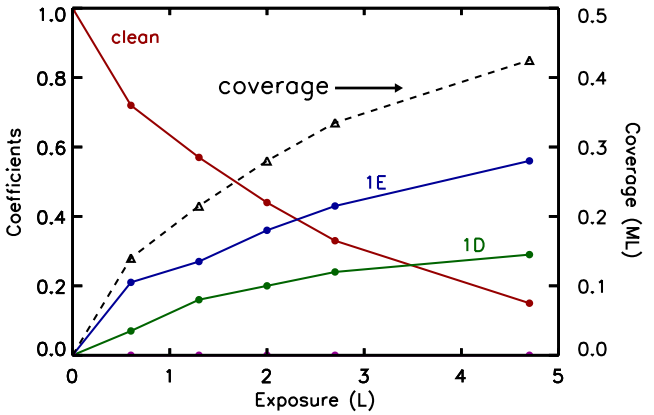

FIG. 6. (Color online) Mixing coefficients (configuration weight) as function of the exposure obtained from the fits shown in Fig. 5 together with the calculated nominal coverage, which can be obtained from the curve of the clean contribution. As the exposure increases, the clean surface contribution decreases in favor of oxidized domains (see text). The weights determined from this graph are used to compute the SDRS in Fig. 7.

reduced at least for the clean surface by the inclusion of excitonic effects.[50] The fitting coefficients, representing the weight of each of the three contributions (1E, 1D, clean), are shown in Fig. 6 as a function of the exposure. The behavior of the coefficients against the exposure is remarkably regular, showing a progressive increase of the 1D and 1E weights. Both the 1D contribution, related to the "oxygen-on-dimers" structure and the 1E one, related to the "oxygen-on-backbonds," saturate at the same rate and appear to follow a Langmuirian law.[51] On the other hand, the clean surface contribution is well visible in the whole range of exposures up to 4.7 L. Between 2 and 3.5 L, the three contributions are comparable, showing that none of the structures alone would be able to reproduce the experimental spectra well.

From the resulting coefficients we can also give an estimate of the effective surface coverage, computed as a weighted sum of the nominal ones, as indicated in Fig. 6. The exponential behavior of oxygen coverage from 0 to 5 L indicates that the initial stages of oxidation follow the Langmuir regime.

D. Low-coverage SDRS

Our previous results, obtained by fitting the RA curves, can now be used to compute SDRS. This represents a good test of the reliability of our procedure since we use mixing coefficients directly taken from Fig. 6. Since in SDR, by definition, the clean surface domains give a null spectrum, our computed spectra read simply as

$$I_{\mathrm{SDR}} = x_D I^{\mathrm{1D}}_{\mathrm{SDR}} + x_E I^{\mathrm{1E}}_{\mathrm{SDR}}, \tag{5}$$

with fixed x_{D} and x_{E} taken from Fig. 6.

The results for SDRS at 1, 2, and 3 L are shown in Fig. 7, in comparison with experimental data. SDRS measured for different gases (on vicinal surfaces) have shown that the main peak at 3.8 eV is typical of the breaking of the dimers, while the peak close to 3 eV characterizes the dangling-bond

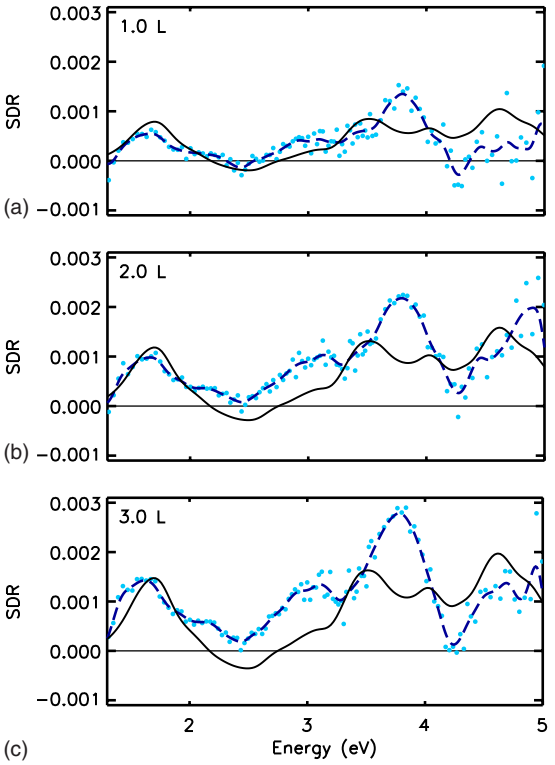

FIG. 7. (Color online) Experimental SDRS (dots and dashed lines) in comparison with theoretical curves obtained from Eq. (5) including the structures 1D+1E (solid line). The mixing coefficients are taken from Fig. 6.

saturation.[10] The agreement is reasonable, with, in particular, a well-reproduced peak at about 1.6 eV, a minimum around 2.5 eV, and a high-energy structure at about 4.7 eV. The results of the "three-component" model are, also for the SDR, better than those which could be achieved by considering single structures alone. It is interesting to notice that the 1.6 eV SDR structure (coming from the dangling-bond to dangling-bond transitions) is mostly arising from the 1E geometrical structure, with oxygen on the back bonds and not in the dimers: this can be explained in terms of dangling-bond electrons captured by oxygen-in-backbond atoms.

E. High-coverage RAS and SDRS

We consider now the RAS and SDRS from surfaces exposed to large amounts of oxygen at room temperature (183 L RAS and 40 and 100 L SDR, respectively) and analyze them on the light of the present calculations. We have checked in other sets of experiments that the SDR spectrum changes very little from 100 to 180 L, and that both exposures correspond to almost the same amount of adsorbed oxygen. A larger exposure (several hundreds or thousands of langmuirs) is needed for a larger oxidation of the surface. The RAS at 183 L is shown in the topmost line in Fig. 3, while the SDRS at 40 and 100 L is displayed in Fig. 8. In fact, Rutherford backscattering experiments on oxidized Si(100) indicate that saturation is reached at a coverage of about 1.5 ML at room temperature, with more than 80% of the oxygen being confined into the topmost Si layer.[16] Moreover, STM shows that already at 15 L the 2×1 dimer structure has vanished, and the local density of states (LDOS) displays an energy gap as large as 1.1 eV, close to the band gap of bulk silicon.[20] *Ab initio* calculations of the band structure of oxidized Si(100) surface at increasing coverage by Fuchs *et al.*[44] showed that at saturation all surface state related bands are pushed out of the region of the Si bulk gap, which explains the observed behavior of the LDOS. It is hence meaningful to compare RAS and SDRS from oxygen-saturated surfaces with our higher-coverage (1.0 to 2.0 ML) structures, namely, C3, C4, and 1G. Since at 4.7 L the main contributions come from the 1D and 1E reconstructions (see Fig. 6), it is reasonable to take into account also these reconstructions.

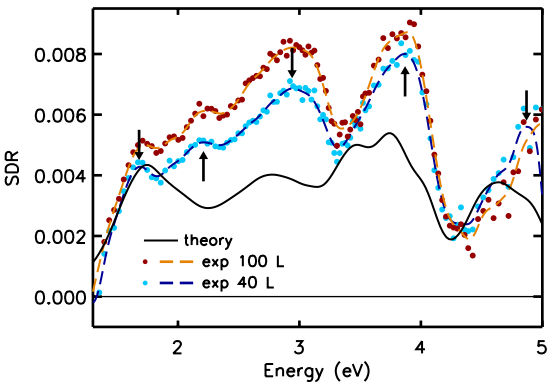

FIG. 8. (Color online) Comparison of the experimental SDR data at high coverage with the theoretical curve obtained from the fit yielding the 1G reconstruction only (solid line). Dark and light dots represent 100 L and 40 L experimental results, respectively. Dashed lines are Gaussian interpolations of the raw data.

The experimental RA signal appears to be almost completely quenched (see Fig. 3). Due to the low intensity of the RA the spectral structure is more affected by noise than in the low-coverage RAS. On the contrary, the experimental SDRS in Fig. 8 shows a clear spectral structure. Furthermore, the intensity increases with increasing oxygen coverage (see Fig. 7). Thus, it is reasonable to go the other way around in the high-coverage case: to fit the SDRS and to extrapolate the RAS. The theoretical SDR spectra considered in the fit are shown in Fig. 9.

We have performed fittings of the 40 L SDR and of the 100 L SDR for various combinations of four reconstructions out of 1D, 1E, C3, C4, and 1G, where also in this case the main experimental peaks as indicated in Fig. 8 are used. The vanishing small RAS at high exposure (see the 183 L curve in Fig. 3) lead us to exclude both C1 and the clean surface from the fit of both SDR shown in Fig. 8. From this procedure we obtain as result for all fits including 1G a unique surface reconstruction: 100% 1G with a coverage of 2.0 ML (see solid line in Fig. 8). From the comparison of the SDRS of these five reconstructions the result is understandable since the 1G shows the largest intensity where the shape of the experimental SDRS is reproduced by 1G and C4. Nevertheless, the resulting coverage of 2.0 ML is slightly larger than the value of 1.5 ML estimated from the experiments,[16] but the reconstruction C4 having the same coverage as the experimental finding does not give the spectral intensity found in the SDR measurement here.

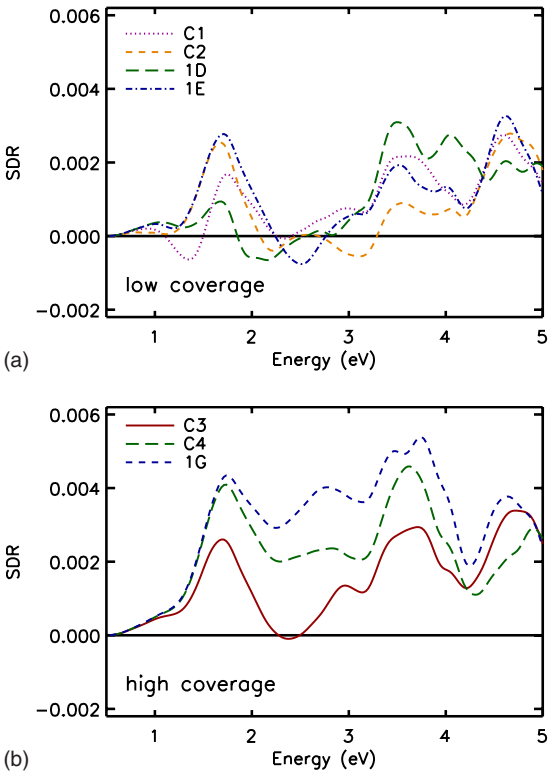

FIG. 9. (Color online) Upper panel: Theoretical SDR of the 0.5 ML coverage structures. Lower panel: Theoretical SDR of structures with oxygen coverage larger than 0.5 ML. (See Fig. 1.)

Inspecting Fig. 8 in detail, we find a good agreement between the shapes of the theoretical and experimental spectra, where most of the features are reproduced. Similar to the low-coverage case we find an underestimation of the region between 2 and 3 eV, which can be traced back to the neglect of excitonic effects.[50] Moreover, it is clear that the calculated curve is underestimating the total intensity experimentally measured. This could be due to the disorder which is present on the real surface induced by the adsorption of oxygen, which likely reduces strongly the surface-related optical transitions. On the contrary, in our calculations, we only consider ordered oxidized surfaces, for which the optical transitions coming from the surface could be less reduced.

Analogous to the way of extrapolating the theoretical SDRS using the coefficients of the fitted RAS, we compare here the "extrapolated" RAS (100% 1G) with the experimental data obtained for 183 L. The corresponding graph is shown in Fig. 10. We find a satisfactory agreement between the theoretical curve and the measured data below 3.5 eV. For higher energies (>3.5 eV) some discrepancies are visible which become stronger as the energy increases. This is because we use a single structure, neglecting in this way disorder. It is well known that hydrogen and oxygen-covered chemical-etched surfaces show a rather strong RA above 3 eV which recently has been explained. This means that some order survives at the surfaces as in the case of the theoretical structure 1G. The disappearing of the experimental RA in Fig. 10 just indicates that we have in the experiment a disordered surface at variance with the 1G in the calculation.

The 1G reconstruction can be achieved by oxidizing the backbonds of the 1D and backbonds and dimers of the 1E reconstruction. In order to give information about the kinetics of this oxidation process, experimental SDR (RAS) spectra for exposures between 5 and 100 L (183 L) are necessary.

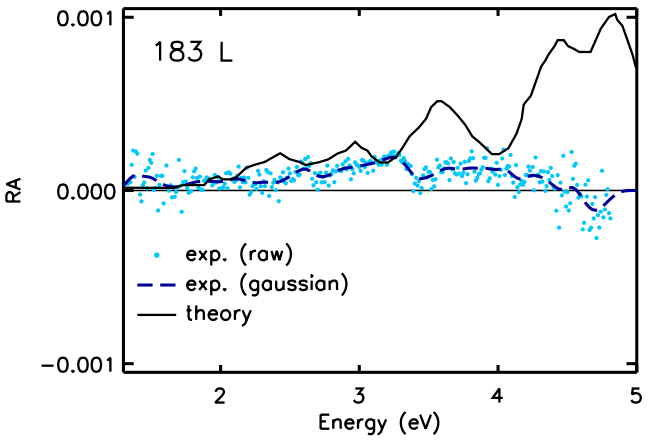

FIG. 10. (Color online) Comparison of the experimental RA data at high coverage (dots and dashed line, the dashed line is the same as in Fig. 3) with the theoretical curve obtained from the fit yielding the 1G reconstruction only (solid line). The dashed line is taken from Fig. 3.

V. CONCLUSIONS

We have studied the first stages of the room-temperature Si(100) surface oxidation by means of surface optical spectroscopy, presenting a comprehensive set of high-quality experimental RA and SDR spectra from small to high experimental coverages and comparing them with theoretical results for a set of low-energy structures. At low exposures ($\leq$5 L) the experimental RAS and SDRS are shown to be consistent with an undersaturated surface, displaying contributions from domains with oxygen occupying the two lowest-energy adsorption sites: Si-Si dimer and dimer backbonds, including a contribution from clean domains. The three relative contributions, estimated by a best fit to the RAS, turn out to vary smoothly with the exposure. Between 2 and 4 L the three contributions are comparable, although the oxygen-on-dimers contribution remains about two times smaller than the oxygen-on-backbonds one. The clean surface contribution vanishes only above $\simeq$5 L, with a nominal coverage approaching 0.5 ML. The calculated coverage is in agreement with the exponential Langmuir rule. Oxygen saturation, which is reached at much higher exposure (40–100 L), yields experimental RAS and SDRS which turn out to be consistent with a surface model having an almost completely oxidized first layer: oxygen is adsorbed on both the dimer backbonds and the Si-Si dimers, yielding a nominal coverage of about 2.0 ML. In the low- (high-) exposure regimes, a consistent description of the experimental SDRS (RAS) is obtained on the basis of the structural contributions determined by fitting the RAS (SDRS). These results definitely improve our understanding of the oxidation mechanism, in which the incorporation of oxygen both on the Si-Si dimers and on Si-Si backbonds has been shown to play a role.

ACKNOWLEDGMENTS

We acknowledge the European Community for financial support under the NANOQUANTA and I3-ETSF project (Contract No. NMP4-CT-2004-500198 and Grant No. 211956). A.I. would like to thank T. Mazza for fruitful discussions. Computer facilities at CINECA granted by INFM (Projects No. 352/2004 and No. 426/2005) and the Supercomputer Center Stuttgart are gratefully acknowledged.

[1] S. Tyagi *et al.*, Tech. Dig. - Int. Electron Devices Meet. 2000, 567 (2000).
[2] D. A. Muller and G. D. Wilk, Appl. Phys. Lett. **79**, 4195 (2001).
[3] L. C. Ciacchi and M. C. Payne, Phys. Rev. Lett. **95**, 196101 (2005).
[4] P. Weightman, D. S. Martin, R. J. Cole, and T. Farrell, Rep. Prog. Phys. **68**, 1251 (2005).
[5] P. Hohenberg and W. Kohn, Phys. Rev. **136**, B864 (1964).
[6] W. Kohn and L. J. Sham, Phys. Rev. **140**, A1133 (1965).
[7] M. Palummo, G. Onida, R. Del Sole, and B. S. Mendoza, Phys. Rev. B **60**, 2522 (1999).
[8] Y. Borensztein, N. Witkowski, and S. Royer, Phys. Status Solidi C **0**, 2966 (2003).
[9] Y. Borensztein and N. Witkowski, J. Phys.: Condens. Matter **16**, S4301 (2004).
[10] Y. Borensztein, O. Pluchery, and N. Witkowski, Phys. Rev. Lett. **95**, 117402 (2005).
[11] N. Witkowski, O. Pluchery, and Y. Borensztein, Phys. Rev. B **72**, 075354 (2005).
[12] O. Pluchery, N. Witkowski, and Y. Borensztein, Phys. Status Solidi B **242**, 2696 (2005).
[13] S. Ohno, H. Kobayashi, F. Mitobe, T. Suzuki, K. Shudo, and M. Tanaka, Phys. Rev. B **77**, 085319 (2008).
[14] E. G. Keim, L. Wolterbeek, and A. Van Silfhout, Surf. Sci. **180**, 565 (1987).
[15] H. Watanabe, K. Kato, T. Uda, K. Fujita, M. Ichikawa, T. Kawamura, and K. Terakura, Phys. Rev. Lett. **80**, 345 (1998).
[16] K. Nakajima, Y. Okazaki, and K. Kimura, Phys. Rev. B **63**, 113314 (2001).
[17] S. Dreiner, M. Schürmann, and C. Westphal, Phys. Rev. Lett. **93**, 126101 (2004).
[18] T.-W. Pi, J.-F. Wen, C.-P. Ouyang, R.-T. Wu, and G. K. Wertheim, Surf. Sci. **478**, L333 (2001).
[19] A. Yoshigoe and Y. Teraoka, Surf. Sci. **532-535**, 690 (2003).
[20] H. Ikegami, K. Ohmori, H. Ikeda, H. Iwano, S. Zaima, and Y. Yasuda, Jpn. J. Appl. Phys., Part 1 **35**, 1593 (1996).
[21] H. Itoh, K. Nakamura, A. Kurokawa, and S. Ichimura, Surf. Sci. **482-485**, 114 (2001).
[22] T. Uchiyama, T. Uda, and K. Terakura, Surf. Sci. **433-435**, 896 (1999).
[23] K. Kato and T. Uda, Phys. Rev. B **62**, 15978 (2000).
[24] N. Richard, A. Estève, and M. Djafari-Rouhani, Comput. Mater. Sci. **33**, 26 (2005).
[25] Y. J. Chabal, K. Raghavachari, X. Zhang, and E. Garfunkel, Phys. Rev. B **66**, 161315(R) 2002.
[26] Y. Widjaja and C. B. Musgrave, J. Chem. Phys. **116**, 5774 (2002).
[27] Y. Hoshino, T. Nishimura, T. Nakada, H. Namba, and Y. Kido, Surf. Sci. **488**, 249 (2001).
[28] H. W. Yeom, H. Hamamatsu, T. Ohta, and R. I. G. Uhrberg, Phys. Rev. B **59**, R10413 (1999).
[29] T. Yasuda, S. Yamasaki, M. Nishizawa, N. Miyata, A. Shklyaev, M. Ichikawa, T. Matsudo, and T. Ohta, Phys. Rev. Lett. **87**, 037403 (2001).
[30] M. A. Albao, D.-J. Liu, M. S. Gordon, and J. W. Evans, Phys. Rev. B **72**, 195420 (2005).
[31] T. Engel, Surf. Sci. Rep. **18**, 93 (1993).
[32] J. B. Hannon, M. C. Bartelt, N. C. Bartelt, and G. L. Kellogg, Phys. Rev. Lett. **81**, 4676 (1998).
[33] M. A. Albao, D.-J. Liu, C. H. Choi, M. S. Gordon, and J. W. Evans, Surf. Sci. **555**, 51 (2004).
[34] R. Shioda and J. van der Weide, Phys. Rev. B **57**, R6823 (1998).
[35] D. E. Aspnes, J. P. Harbison, A. A. Studna, and L. T. Florez, J. Vac. Sci. Technol. A **6**, 1327 (1988).
[36] Y. Borensztein, T. Lopez-Rios, and G. Vuye, Appl. Surf. Sci. **41-42**, 439 (1989).
[37] G. Onida, L. Reining, and A. Rubio, Rev. Mod. Phys. **74**, 601 (2002).
[38] F. Fuchs, W. G. Schmidt, and F. Bechstedt, Phys. Rev. B **72**, 075353 (2005).
[39] R. Del Sole and R. Girlanda, Phys. Rev. B **48**, 11789 (1993).
[40] F. Manghi, R. Del Sole, A. Selloni, and E. Molinari, Phys. Rev. B **41**, 9935 (1990).
[41] R. Del Sole, in *Photonic Probes of Surfaces*, edited by P. Halevi (Elsevier, Amsterdam, 1995), p. 131.
[42] O. Pulci, G. Onida, R. Del Sole, and A. J. Shkrebtii, Phys. Rev. B **58**, 1922 (1998).
[43] A. Incze, R. Del Sole, and G. Onida, Phys. Rev. B **71**, 035350 (2005).
[44] F. Fuchs, W. G. Schmidt, and F. Bechstedt, J. Phys. Chem. B **109**, 17649 (2005).
[45] K. Kato, T. Uda, and K. Terakura, Phys. Rev. Lett. **80**, 2000 (1998).
[46] N. Takahashi, Y. Nakamura, J. Nara, Y. Tateyama, T. Uda, and T. Ohno, Surf. Sci. **602**, 768 (2008).
[47] T. Yamasaki, K. Kato, and T. Uda, Phys. Rev. Lett. **91**, 146102 (2003).
[48] S. G. Jaloviar, J.-L. Lin, F. Liu, V. Zielasek, L. McCaughan, and M. G. Lagally, Phys. Rev. Lett. **82**, 791 (1999).
[49] J. R. Power, O. Pulci, A. I. Shkrebtii, S. Galata, A. Astropekakis, K. Hinrichs, N. Esser, R. Del Sole, and W. Richter, Phys. Rev. B **67**, 115315 (2003).
[50] M. Palummo, R. Del Sole, N. Witkowski, and Y. Borenzstein (unpublished).
[51] N. Witkowski, K. Gaál-Nagy, F. Fuchs, O. Pluchery, A. Incze, F. Bechstedt, Y. Borensztein, G. Onida, and R. Del Sole, Eur. Phys. J. B **66**, 427 (2008).